

June, 1980

ERC41033.25TPR

ADVANCED PHOTOVOLTAIC CONCENTRATOR CELLS

Quarterly Technical Progress Report No. 3  
for period 03/1/80 through 5/31/80

By

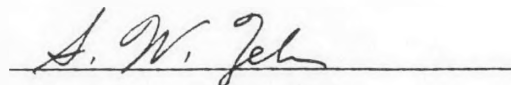
H. T. Yang, J. J. J. Yang and S. W. Zehr  
Rockwell International Electronics Research Center  
Thousand Oaks, California 91360  
\*Anaheim, California 92803

For

Solar Energy Research Institute  
Photovoltaics Program Office  
PVPO - Documentation  
1617 Cole Boulevard  
Golden, Colorado 80401

Prepared under Contract No. XJ-9-8058-2

Approved by:



S. W. Zehr  
Program Manager

## **DISCLAIMER**

**This report was prepared as an account of work sponsored by an agency of the United States Government. Neither the United States Government nor any agency thereof, nor any of their employees, makes any warranty, express or implied, or assumes any legal liability or responsibility for the accuracy, completeness, or usefulness of any information, apparatus, product, or process disclosed, or represents that its use would not infringe privately owned rights. Reference herein to any specific commercial product, process, or service by trade name, trademark, manufacturer, or otherwise does not necessarily constitute or imply its endorsement, recommendation, or favoring by the United States Government or any agency thereof. The views and opinions of authors expressed herein do not necessarily state or reflect those of the United States Government or any agency thereof.**

---

## **DISCLAIMER**

**Portions of this document may be illegible in electronic image products. Images are produced from the best available original document.**

## TABLE OF CONTENTS

	<u>Page</u>
1.0 INTRODUCTION.....	1
2.0 MODELING.....	3
3.0 MATERIALS DEVELOPMENT.....	7
3.1 Accomplishments.....	7
3.2 AlGaAs Subcells.....	7
3.3 AlGaSb Subcells.....	8
3.4 Intercell Ohmic Contacts (IOCs) and Bonding.....	12
4.0 DEVICE FABRICATION AND CHARACTERIZATION.....	22
4.1 Accomplishments.....	22
4.2 AlGaSb Subcells.....	22
4.3 AlGaAs Subcells.....	28

## LIST OF FIGURES

	<u>Page</u>
Fig. 1. Comparison of measured and calculated spectral responses for AlGaAs subcells.....	4
Fig. 2. Comparison of measured and calculated spectral responses for an AlGaSb heteroface subcell having 40 mole % AlSb in the window layer and 20 mole % AlSb in the junction layers. .	6
Fig. 3. Comparison of spectral responses from nominal Al <sub>0.35</sub> Ga <sub>0.65</sub> As subcell structures grown by (a) conventional interrupted MO-CVD growth, (b) continuous MO-CVD growth, and (c) MBE growth.....	9
Fig. 4. Surface morphology of etched back layers and Ga inclusion of GaSb and Al <sub>0.65</sub> Ga <sub>0.35</sub> AsSb on GaSb substrate.....	10
Fig. 5. Smoother surfaces produced by equilibrating system at the growth temperature for several minutes prior to beginning growth.....	11
Fig. 6. Non-uniform nucleation of Al <sub>0.4</sub> Ga <sub>0.6</sub> AsSb on GaSb substrate... .	13
Fig. 7. Smooth growth of Al <sub>0.4</sub> Ga <sub>0.6</sub> AsSb on GaSb substrate.....	14
Fig. 8. Device structure diagrams of heteroface and shallow homo-junction solar cell.....	15
Fig. 9. Spectral response curves of heteroface structure with same junction layers but different window layers.....	16
Fig. 10. Spectral response curves of AlGaSb heteroface structures with different junction layers but same window layers.....	17
Fig. 11. Spectral response curves of an Al <sub>0.2</sub> Ga <sub>0.8</sub> Sb heteroface cell with 65% Al window layer and an Al <sub>0.2</sub> Ga <sub>0.8</sub> Sb shallow homo-junction cell.....	18
Fig. 12. Current voltage characteristics of (a) ITO/p <sup>+</sup> Al <sub>0.65</sub> Ga <sub>0.35</sub> AsSb and (b) ITO/n <sup>+</sup> GaAs contacts.....	20
Fig. 13a Light I-V curve for p <sup>+</sup> Al <sub>0.65</sub> Ga <sub>0.35</sub> AsSb/p Al <sub>0.2</sub> Ga <sub>0.8</sub> Sb/n Al <sub>0.2</sub> Ga <sub>0.8</sub> Sb/n GaSb heteroface cell under simulated 1 SUN AM1 illumination. Front contact made directly to window layer.	24



## LIST OF FIGURES (Cont.)

	<u>Page</u>
Fig. 13b. Light I-V curve for $p^+$ $Al_{1.4}Ga_{0.6}AsSb/p$ $Al_{1.2}Ga_{0.8}Sb/n$ $Al_{1.2}Ga_{0.2}Sb/n$ GaSb heteroface cell under simulated 1 SUN AM1 illumination. Front contact made directly to window layer.....	25
Fig. 14. Light I-V curves for $p^+$ $Al_{1.2}Ga_{0.8}Sb/n$ $Al_{1.2}Ga_{0.8}Sb$ shallow homojunction cell under simulated 1 SUN and $\sim 200$ SUNs illumination.....	26
Fig. 15. Open circuit voltage vs. time under a camera flash unit simulated $\sim 1000$ SUNs illumination.....	27
Fig. 16. Light I-V curve for $p^+$ $Al_{1.85}Ga_{0.15}As/p$ $Al_{1.35}Ga_{0.65}As/n$ $Al_{1.35}Ga_{0.65}As/n$ GaAs cell under simulated 1 SUN AM1 illumination. Unalloyed Au-Zn front contact applied directly to junction layer.....	29
Fig. 17. Dark I-V curves for $p^+$ $Al_{1.85}Ga_{0.15}As/p$ $Al_{1.35}Ga_{0.65}As/n$ $Al_{1.35}Ga_{0.65}As/n$ GaAs cell before and after alloying process.	30



## ABSTRACT

This report describes third quarter activities for a project aimed at demonstrating the technical feasibility of advanced high efficiency concentrator solar converters. The goal of the program is to achieve 30% conversion efficiency with a converter operating at 30°C under 500-1000 SUNs AM2 illumination and 25% conversion efficiency with a converter operating at 150°C under 500-1000 SUNs AM2 illumination. The approach is to fabricate two cell, non-lattice matched, monolithic stacked converters using optimum pairs of cells having bandgaps in the range of 1.6-1.7 eV and 0.95-1.1 eV. The high bandgap subcells are to be fabricated using MO-CVD or LPE to produce the needed AlGaAs layers of optimized composition, thickness and doping to produce high performance, heteroface homojunction devices. The low bandgap subcells are to be similarly fabricated from AlGaSb(As) compositions by LPE. These subcells are then to be joined into a monolithic structure by an appropriate thermal bonding technique which will also form the needed transparent intercell ohmic contact (IOC) between the two subcells.

The low bandgap subcell development activities have continued during this quarter. In addition, a problem of poor blue response observed for AlGaAs high bandgap cells grown by MO-CVD has been addressed and solved. The Nd-glass pulsed laser for bonding has been received and is being made operational.

## 1.0 INTRODUCTION

Within the last several years, there has been growing interest in exploiting the significantly improved levels of power conversion efficiency which are theoretically available from multibandgap solar photovoltaic converters<sup>(1-5)</sup>. This interest has been sparked by the recognition that even a partial realization of these potential performance gains can provide significant leverage for reduction of the cost of output electric power from concentrator photovoltaic systems<sup>(6)</sup>.

Upper bound conversion efficiencies near 40% and 47% have been calculated for optimum bandgap two and three junction converters respectively operating at 300° K under terrestrial sunlight concentrated to several hundred to one thousand SUNs<sup>(1-5)</sup>. Even when practical losses are taken into account, such converters offer a reasonable prospect for achieving at least 30% efficiency from stacked, monolithic, two-bandgap structures of well-optimized design, operating at 30°C under 500-1000 SUNs AM2 illumination.

Such devices also offer the option of operating at these levels of sunlight concentration at moderately elevated temperatures (~150°C) with at least 25% electrical conversion efficiency and the added bonus of providing usable quality heat for total energy applications.

It is the objective of this project to demonstrate the technical feasibility of producing monolithic stacked multibandgap solar cells having 30% conversion efficiency at 30°C and 25% conversion efficiency at 150°C under 500-1000 SUNs AM2 illumination.

To meet this objective, the following tasks will be performed:

1. Grow and optimize single junction AlGaAs cells having bandgaps of 1.6 eV and 1.7 eV and AlGaSb cells having bandgaps of 0.95 eV and 1.1 eV.
2. Develop techniques for joining these optimized single junction cells by means of non-lattice matched intercell ohmic contacts



ERC41033.25TPR

having sufficient optical transparency combined with low electrical and thermal resistance to meet the overall performance objective.

3. Characterize performance of the individual cells and stacked combinations using appropriate light and dark I-V and spectral response measurements over the operating temperature range of 30-200°C and for illumination levels of 1-1000 SUNs AM2.

## 2.0 MODELING

Attempts have been made this quarter to match spectral response curves and corresponding reflection-corrected values of short circuit current densities measured from typical subcells with results calculated from the computer model.

In Fig. 1, measured and calculated spectral response curves for a typical LPE grown AlGaAs heteroface subcell structure are compared with the calculated curve for the initial optimized AlGaAs subcell structure (see quarterly report #1) for the multicolor converter. The measured and reflection corrected value of short circuit current density,  $J_{SC}$ , for the experimental cell is noted in the figure along with the  $J_{SC}$  corresponding to the two calculated curves. The structure and device parameters measured and assumed for generation of the curves of Fig. 1 are summarized in Table I. It can be seen that the various sets of parameter values, the  $J_{SC}$  values and the spectral response curves are quite self consistent.

In Fig. 2, a similar comparison is made of the measured and calculated spectral response curves for a 40% Al window layer, 20% Al junction layer AlGaSb subcell structure. Again the detailed agreement is quite good between the two curves. The measured and reflection-corrected value of  $J_{SC} = 6.9 \text{ mA/cm}^2$  is in good agreement with the calculated value of  $6.83 \text{ mA/cm}^2$  for 1 SUN AM2. The apparent displacement between the two curves is no more than the uncertainty of the bandgap dependence of optical absorption associated with our available data for the AlGaSb alloy system. The assumed values of minority carrier diffusion lengths which provided the matching calculated spectral response curve ( $L_n = 2.5 \text{ } \mu\text{m}$  in the p-layer and  $L_p = 1.0 \text{ } \mu\text{m}$  in the n-layer) are reasonably consistent with recently measured values of  $L_n = L_p = 1.4 \text{ } \mu\text{m}$  obtained by EBIC. The EBIC values may be underestimated due to surface recombination effects. The accelerating voltage used was only 20 keV. We intend to make further measurements over a range of higher voltages to explore this possibility.

ERC41033.25TPR

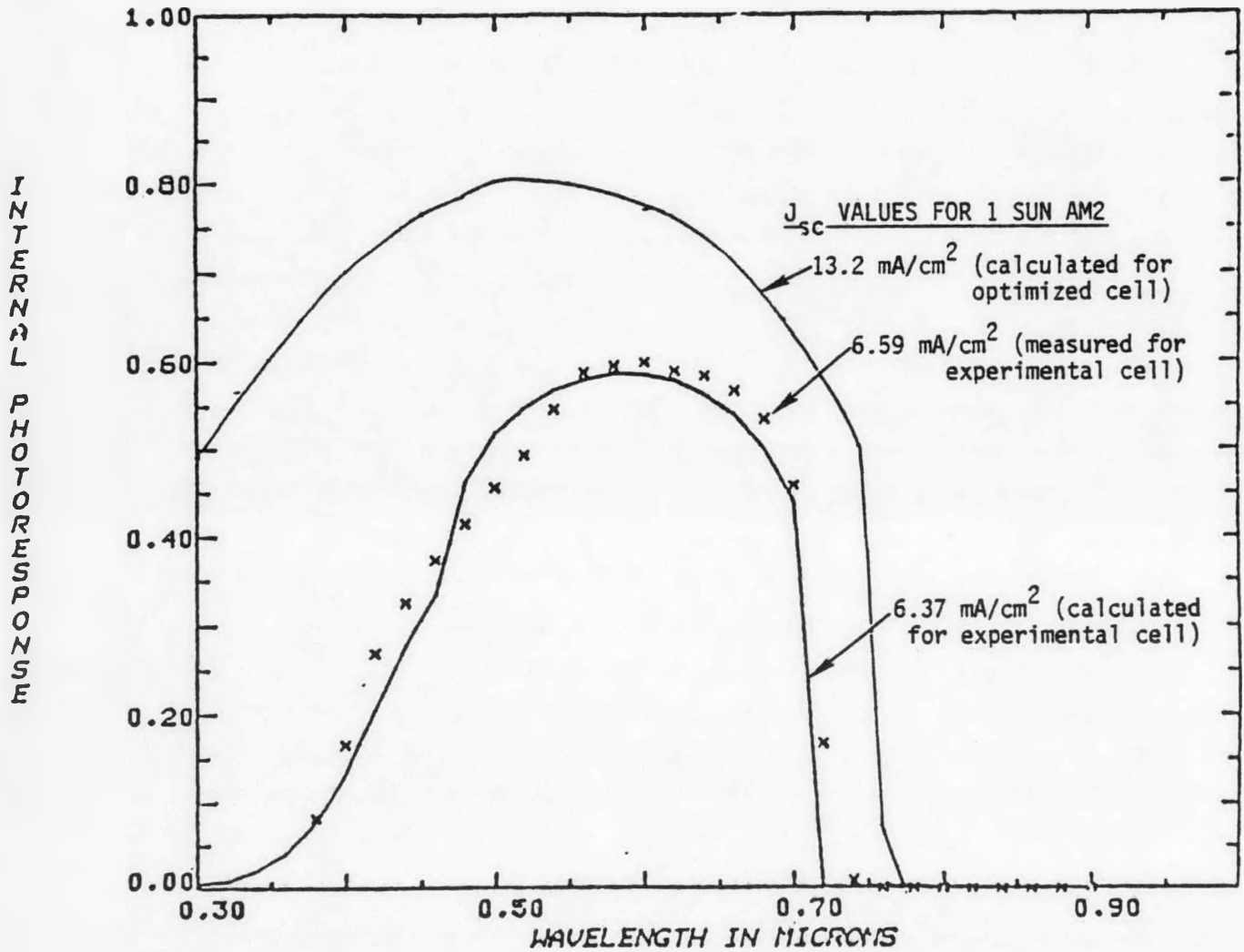


Fig. 1. Comparison of measured and calculated spectral responses for AlGaAs subcells.

TABLE I  
SUMMARY OF STRUCTURE AND DEVICE PARAMETERS FOR AlGaAs SUBCELL  
SPECTRAL RESPONSE CALCULATIONS AND MEASUREMENTS SHOWN IN Fig. 1

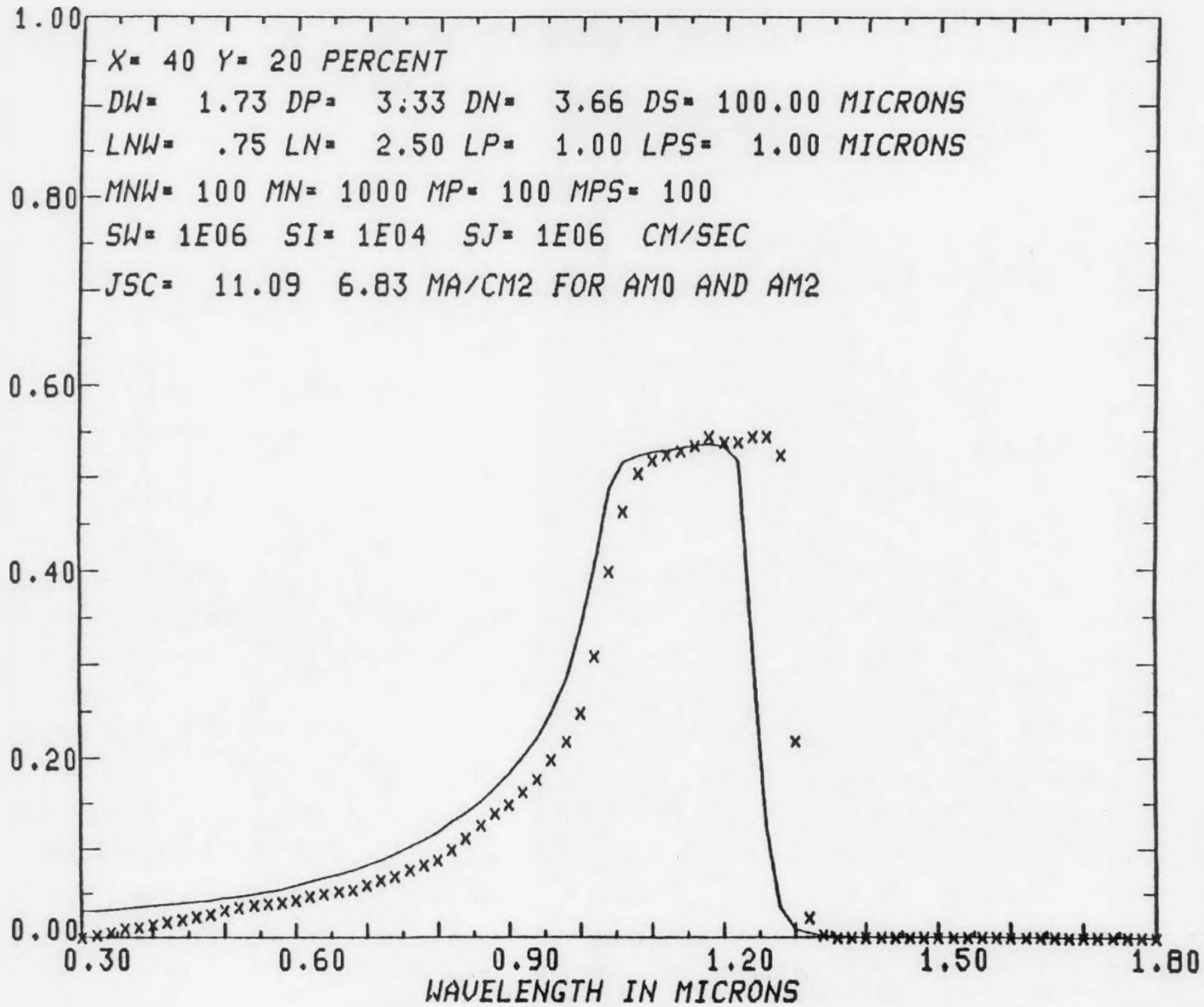
PARAMETER	VALUE FOR CALCULATED OPTIMUM AlGaAs SUBCELL	VALUE USED TO MATCH EXPERIMENTAL CELL RESULTS	VALUE MEASURED FROM EXPERIMENTAL CELL
Junction Layer Al Fraction	0.2	0.24	---
Junction Layer Bandgap (eV)	1.65 eV	1.75	1.75
p-Layer Thickness ( $\mu\text{m}$ )	0.5	0.7	0.7
Window Layer Al Fraction	0.85	0.80	---
Window Layer Bandgap (eV)	2.1 Indirect.	2.05 Indirect	---
Window Layer Thickness ( $\mu\text{m}$ )	0.1	0.57	0.57
Assumed $L_n$ in Window Layer ( $\mu\text{m}$ )	0.05	0.1	---
Assumed $L_n$ in p-layer ( $\mu\text{m}$ )	0.7	0.7	---
Assumed $L_p$ in n-layer ( $\mu\text{m}$ )	0.5	0.5	---
Assumed Interface Recombination Velocity (cm/sec)	$10^4$	$10^3$	---
Assumed Surface Recombination Velocity (cm/sec)	$10^6$	$10^6$	---
Assumed mobility (all layers) ( $\text{cm}^2/\text{V}\cdot\text{sec}$ )	250	250	---
Reflection Corrected Short Circuit Current Density 1 SUN AM2 ( $\text{A}/\text{cm}^2$ )	$13.2 \times 10^{-3}$	$7.36 \times 10^{-3}$	$6.59 \times 10^{-3}$

ERC41033.25TPR



Rockwell International

INTERNAL PHOTORESPONSE



ERC41033.25TPR



Rockwell International

Fig. 2. Comparison of measured and calculated spectral responses for an AlGaSb heteroface subcell having 40 mole % AlSb in the window layer and 20 mole % AlSb in the junction layers.

### 3.0 MATERIALS DEVELOPMENT

#### 3.1 Accomplishments

- The growth problems (etchback and non-wetting) of AlGaSb were solved in this period.
- Heteroface AlGaSb solar cell structures covering a wide range of Al content in either window layers or junction layers have been grown.
- p<sup>+</sup>/n shallow homojunction AlGaSb solar cell structures were grown.
- Improved blue response has been achieved in AlGaAs cells using MBE growth and graded bandgap MO-CVD continuous growth.

#### 3.2 AlGaAs Subcells

Recent results on AlGaAs subcells grown by MO-CVD as part of our companion Air Force stacked cell program have revealed a serious deficiency in short wavelength response ( $\lambda < 0.60 \mu\text{m}$ ) from these devices. The cause was postulated to be the presence of a high density of trapping states at the window layer/p-junction layer interface. It is believed that the presence of these states leads to an unacceptably high value for interface recombination velocity which accounts for the observed poor blue response. The source of these trapping states at the interface is currently believed to be low level oxygen or moisture contamination of the MO-CVD growth system which leads to slight but significant oxidation of the exposed AlGaAs surface during pauses in growth to allow changes in composition and/or doping. These pauses have been routine process steps in the past to allow flushing of previous dopants and alloying reactants prior to beginning growth of a new layer of different composition.

Two approaches to solving this problem are being pursued in parallel. One approach is to grow AlGaAs subcells by MBE. The other is to develop a continuous MO-CVD growth procedure which allows no opportunity for interface oxidation.

Preliminary MBE and continuous growth MO-CVD Al<sub>0.35</sub>Ga<sub>0.65</sub>As subcell structures have been produced and subjected to spectral response measurements. Both types of structures exhibit marked improvement in blue response over the conventionally grown MO-CVD AlGaAs subcells reported previously. The normalized spectral responses for typical MBE, continuously grown MO-CVD and conventionally grown MO-CVD structures are compared in Fig. 3. (This figure has also been reported as relevant to the Air Force stacked cell program.) It appears that the loss of blue response tentatively attributed to a high interface-state density in the conventionally grown MO-CVD structures has been significantly reduced using both of the two alternative growth techniques. There appears to be room for further blue response improvement even in these alternative structures through reduction of the high reflectivity at wavelengths shorter than  $\sim 0.45 \mu\text{m}$ . This, combined with relatively short diffusion lengths in the AlGaAs layers, is thought to be the origin of the remaining collection losses in the blue. The reflection losses can be easily corrected with proper AR coatings. It is presently not clear how to most effectively improve p-layer diffusion lengths in this material.

### 3.3 AlGaSb Subcells

As mentioned in the last quarterly report, etchback and non-wetting of the substrate have been our main problems of growth of AlGaSb subcells. Figure 4 shows growth surfaces which were etched back by the melt, and the inclusion of Ga in some of them. For the example GaSb layers, etchback was a result of undersaturation. For the high Al content ternary layers, even several degrees of supersaturation was found to be insufficient to prevent etchback as can be seen from the micrographs of Fig. 4. It was later found that by holding at the growth temperature for a couple of minutes before beginning growth, better morphology could be obtained (Fig. 5).



ERC41033.25TPR

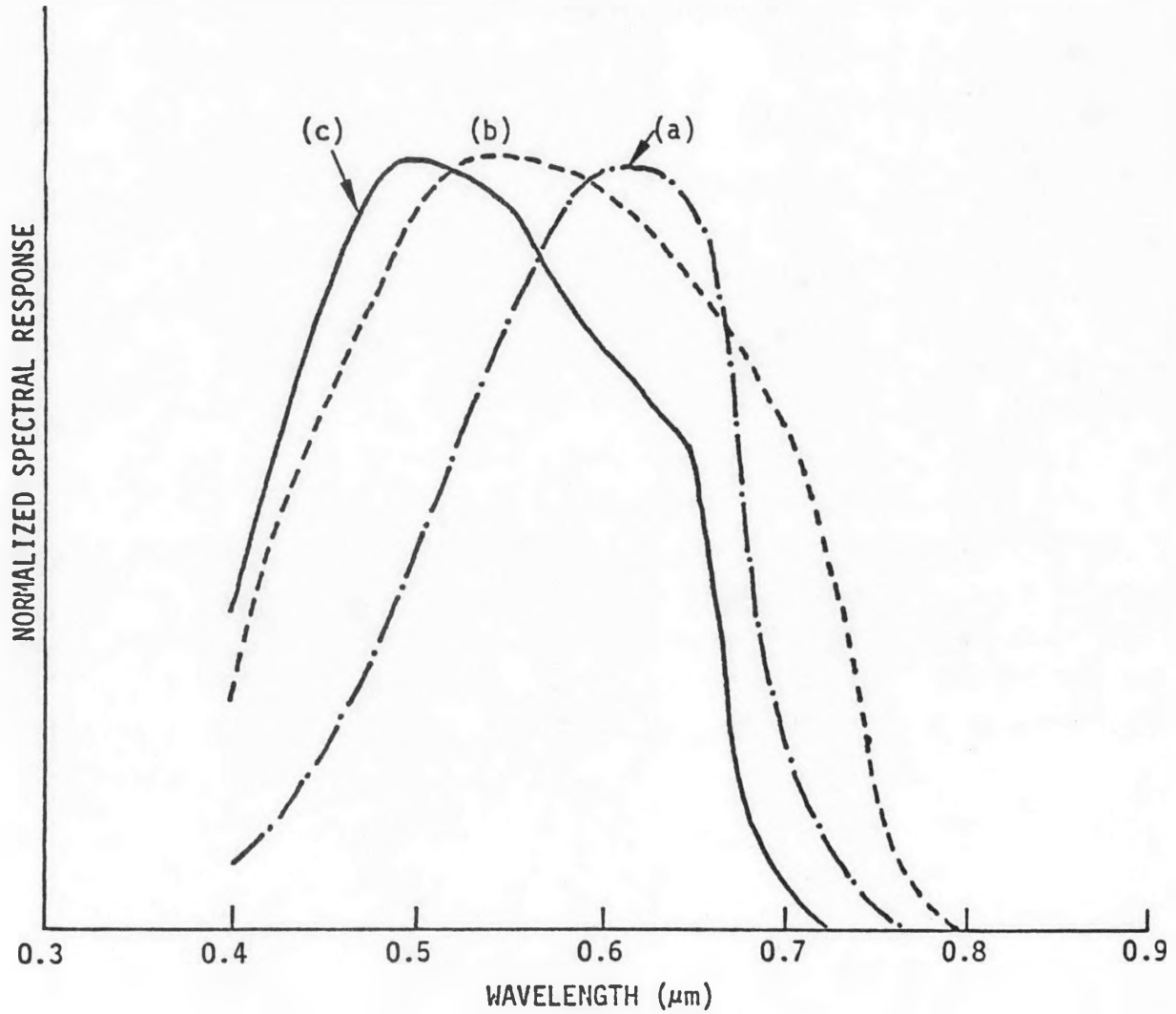
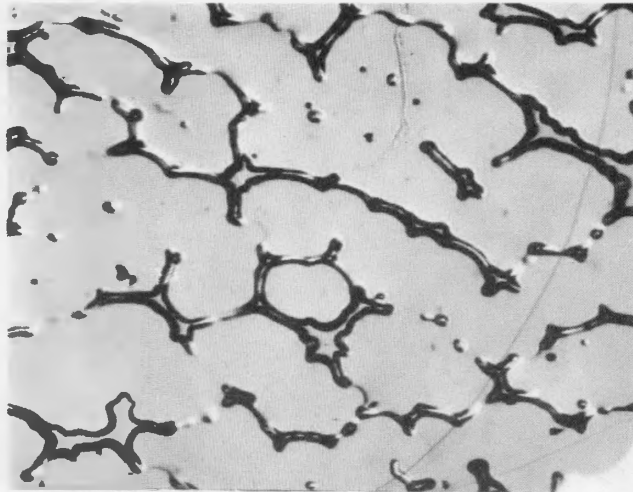


Fig. 3. Comparison of spectral responses from nominal Al<sub>1-x</sub>Ga<sub>x</sub>As subcell structures grown by (a) conventional interrupted MO-CVD growth, (b) continuous MO-CVD growth, and (c) MBE growth.



GaSb/GaSb

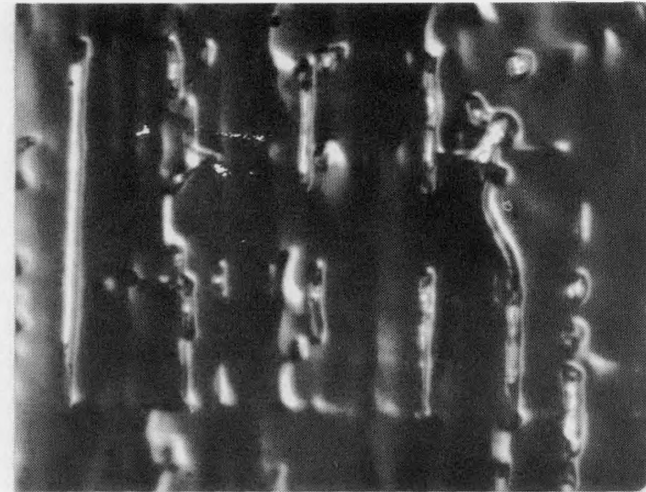
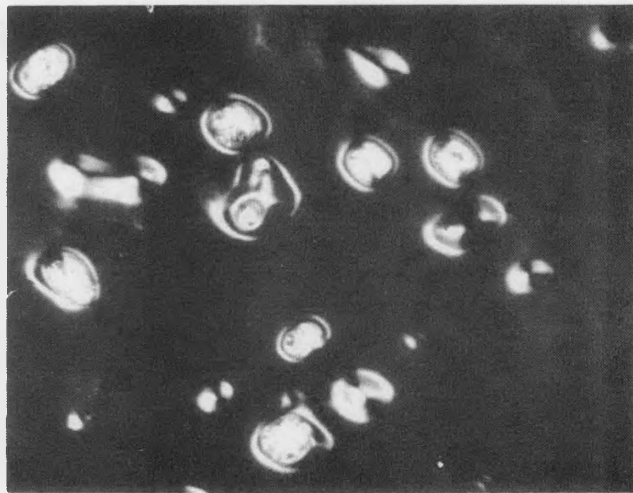
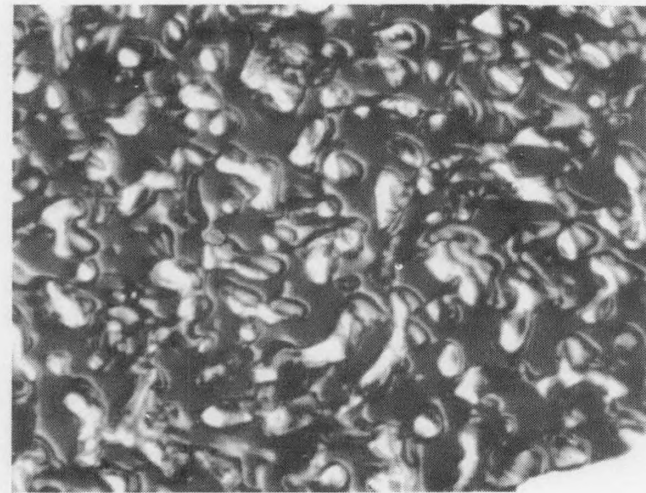
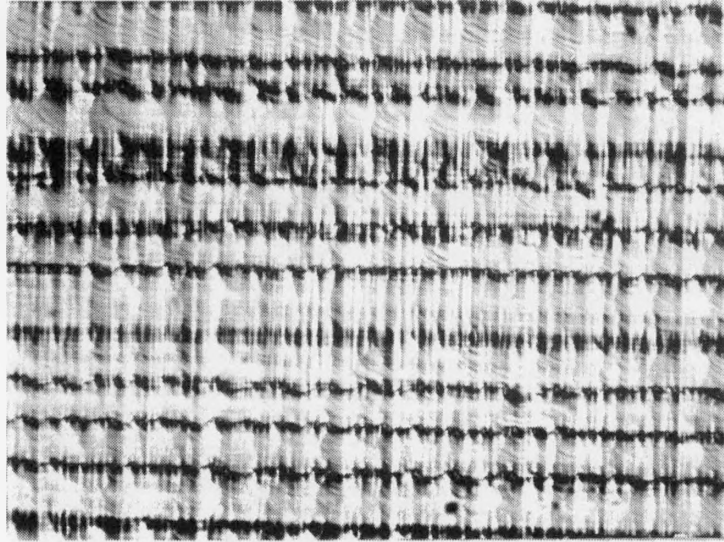
 $\text{Al}_{.65}\text{Ga}_{.35}\text{AsSb}/\text{GaSb}$  $\text{Al}_{.65}\text{Ga}_{.35}\text{AsSb}/\text{GaSb}$  $\text{Al}_{.65}\text{Ga}_{.35}\text{AsSb}/\text{GaSb}$ 

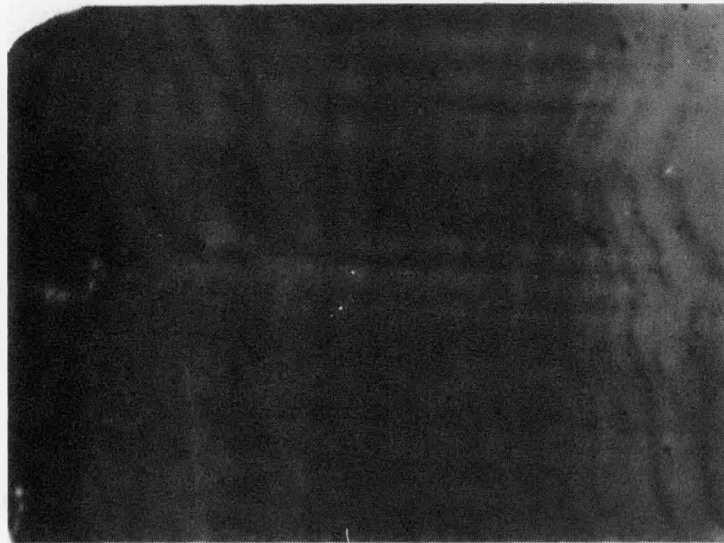
Fig. 4 Surface morphology of etched back layers and Ga inclusion of GaSb and  $\text{Al}_{.65}\text{Ga}_{.35}\text{AsSb}$  on GaSb substrate.

ERC80-8636



x40

Al<sub>.65</sub>Ga<sub>.35</sub>AsSb/GaSb



x400

Al<sub>.65</sub>Ga<sub>.35</sub>AsSb/GaSb

Fig. 5 Smoother surfaces produced by equilibrating system at the growth temperature for several minutes prior to beginning growth.

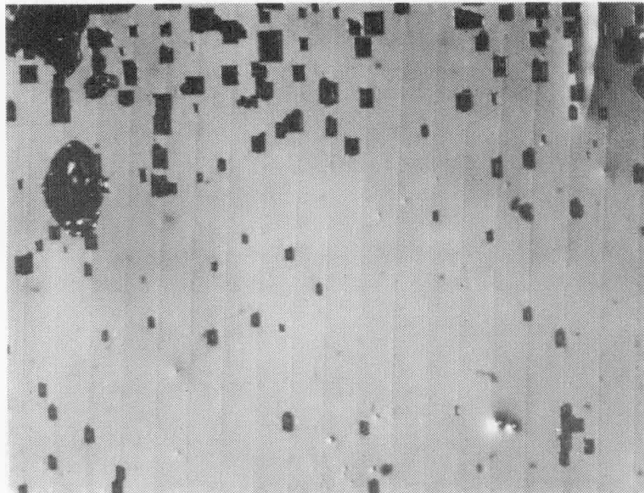
Figure 6 is typical of cases where the melt did not wet some of the areas of the substrates causing spotty nucleation. This kind of nucleation and growth leads to Ga entrapment and layer discontinuity. The cause of this non-uniform nucleation is contamination of either the substrate or the melt. The source of contamination is either improper substrate preparation or a leak in the growth system. Subsequent cleaning of the growth system and efforts to eliminate possible leaks has resulted in smooth and continuous growth being routinely obtained (Fig. 7).

Following solution of these growth problems, a series of heteroface cell structures with Al content varied over a wide range in both the window layer and junction layers have been successfully grown (Fig. 8). The spectral response curves for these structures are shown in Figs. 9-11.

Some  $\text{Al}_{.2}\text{Ga}_{.8}\text{Sb}$  homojunctions having no window layers were also grown, fabricated and characterized. The preliminary spectral response results suggest that window layers may not be necessary for subcells of this material having reasonably shallow junctions ( $\leq 0.3 \mu\text{m}$ ). In Fig. 11, a typical spectral response curve from one of the windowless shallow homojunction structures is compared with the response of a heteroface structure having a 65% Al window layer grown from a saturated As solution. The improved short wavelength response of the shallow homojunction structure is quite evident.

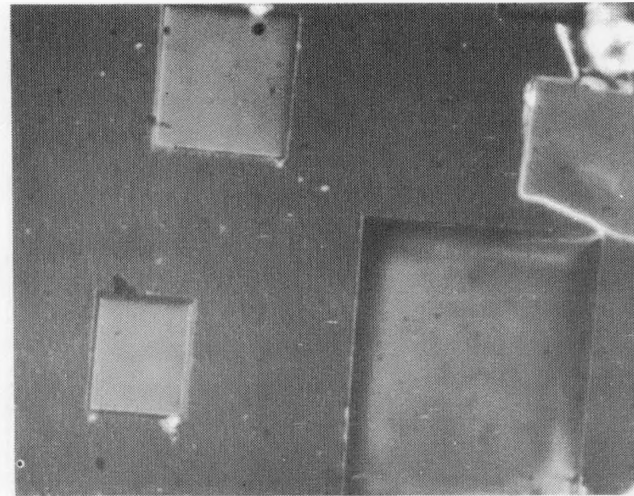
### 3.4 Intercell Ohmic Contacts (IOCs) and Bonding

ITO films have been deposited on different  $\text{AlGaSb}$ ,  $\text{AlGaAs}$  and  $\text{GaAs}$  samples (see Table II) by ion beam sputtering techniques at Colorado State University. Mesa dots have been made on those films using In-Au as a contact alloy. Only the  $\text{ITO}/\text{p}^+ \text{Al}_{.65}\text{Ga}_{.35}\text{AsSb}$  showed ohmic behavior. The others were all soft diodes (see Fig. 12). Annealing at  $400^\circ\text{C}$  for 5 min. did not improve the results. Also, some loss of ITO by evaporation was apparent during alloying at this temperature.



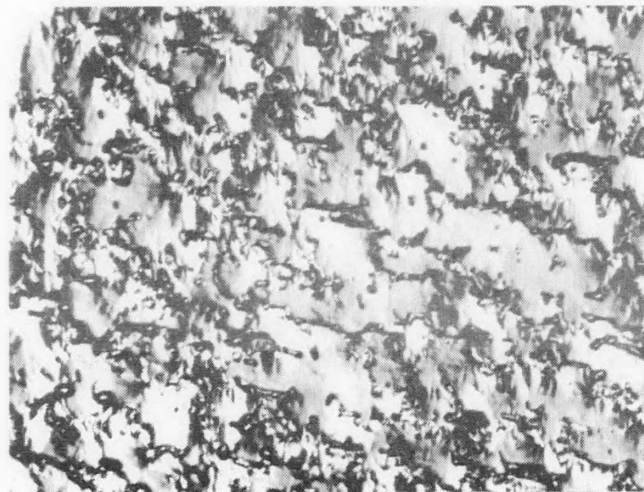
Al<sub>0.4</sub>Ga<sub>0.6</sub>AsSb/GaSb

x40



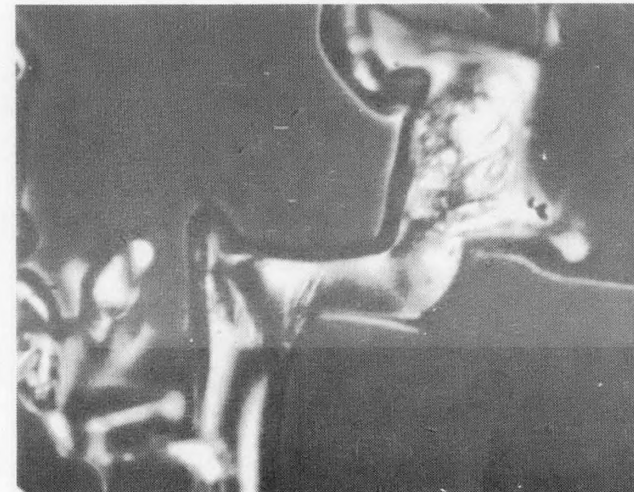
x400

Al<sub>0.4</sub>Ga<sub>0.6</sub>AsSb/GaSb



Al<sub>0.4</sub>Ga<sub>0.6</sub>AsSb

x40

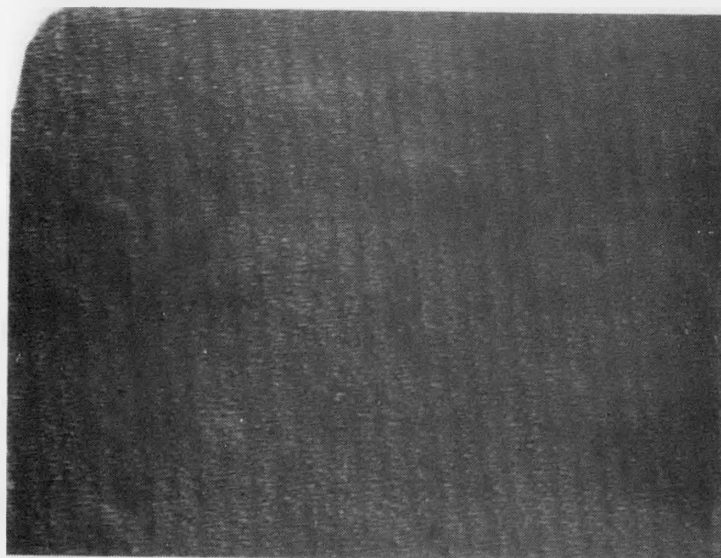


x400

Al<sub>0.4</sub>Ga<sub>0.6</sub>AsSb/GaSb

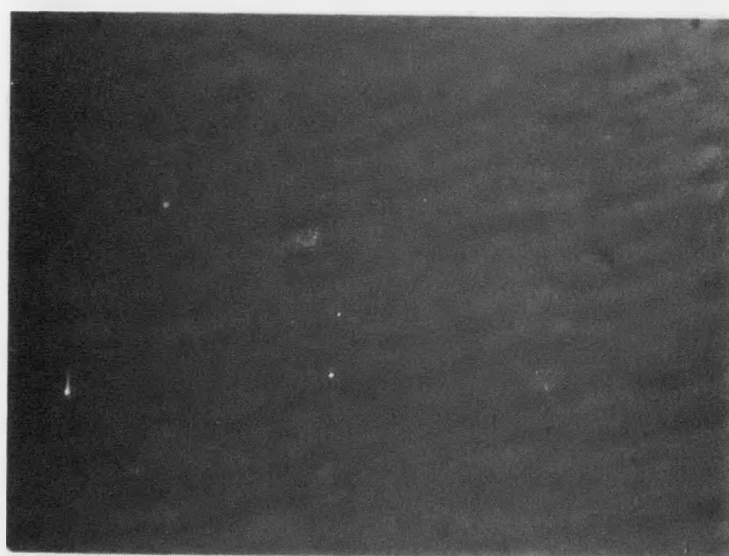
Fig. 6 Non-uniform nucleation of Al<sub>0.4</sub>Ga<sub>0.6</sub>AsSb on GaSb substrate.

ERC80-8632



x40

Al<sub>.4</sub>Ga<sub>.6</sub>AsSb/GaSb



x400

Al<sub>.4</sub>Ga<sub>.6</sub>AsSb/GaSb

Fig. 7 Smooth growth of Al<sub>.4</sub>Ga<sub>.6</sub>AsSb on GaSb substrate.

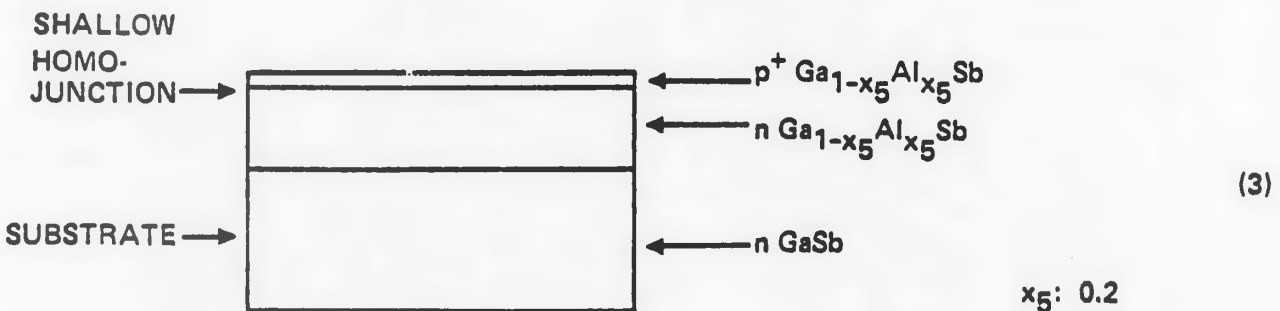
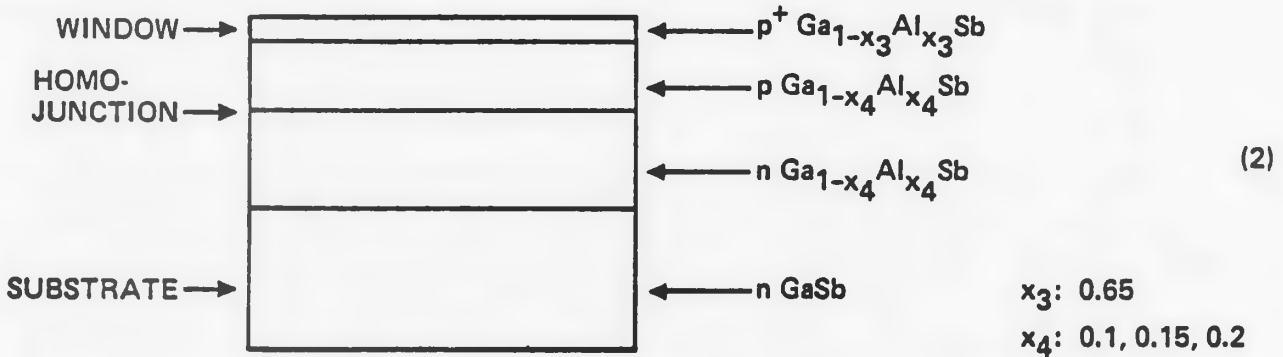
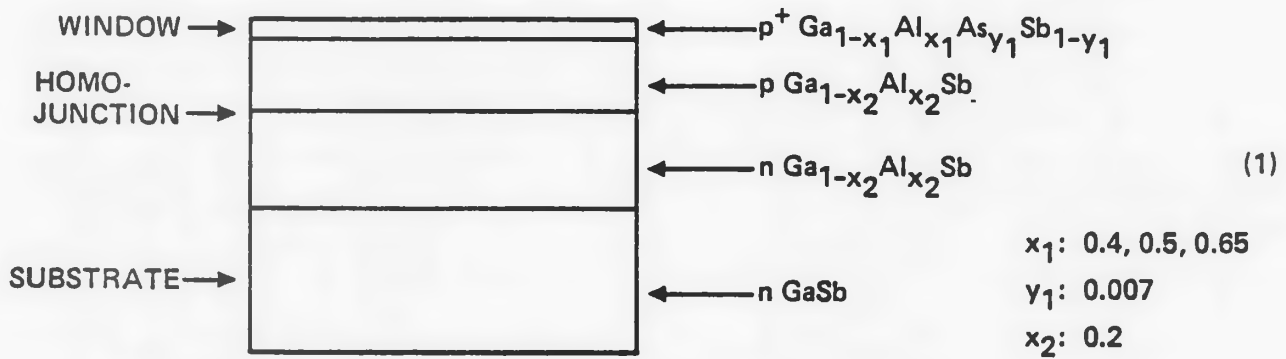
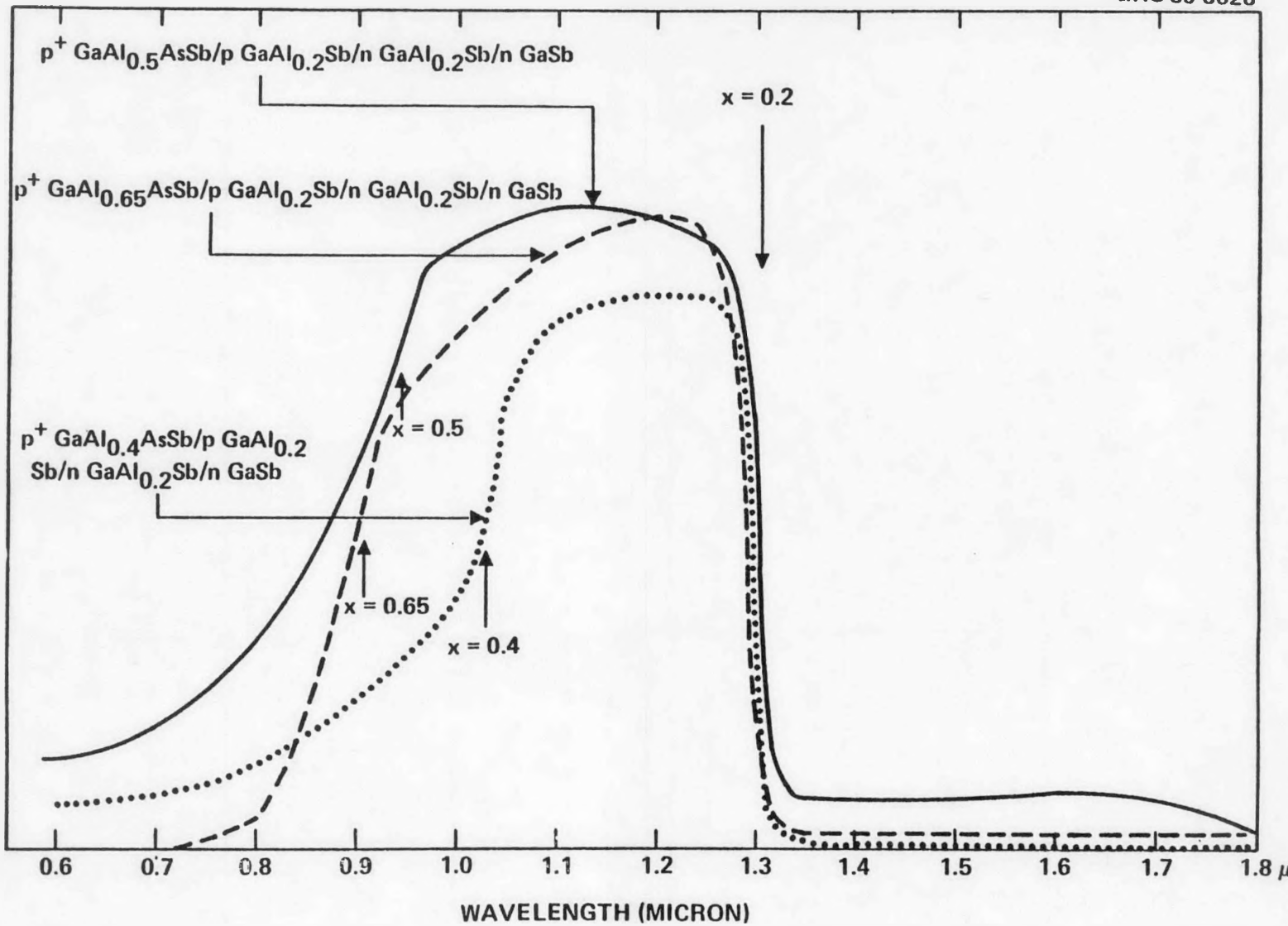


Fig. 8. Device structure diagrams of heteroface and shallow homojunction solar cell.

ARBITRARY UNIT



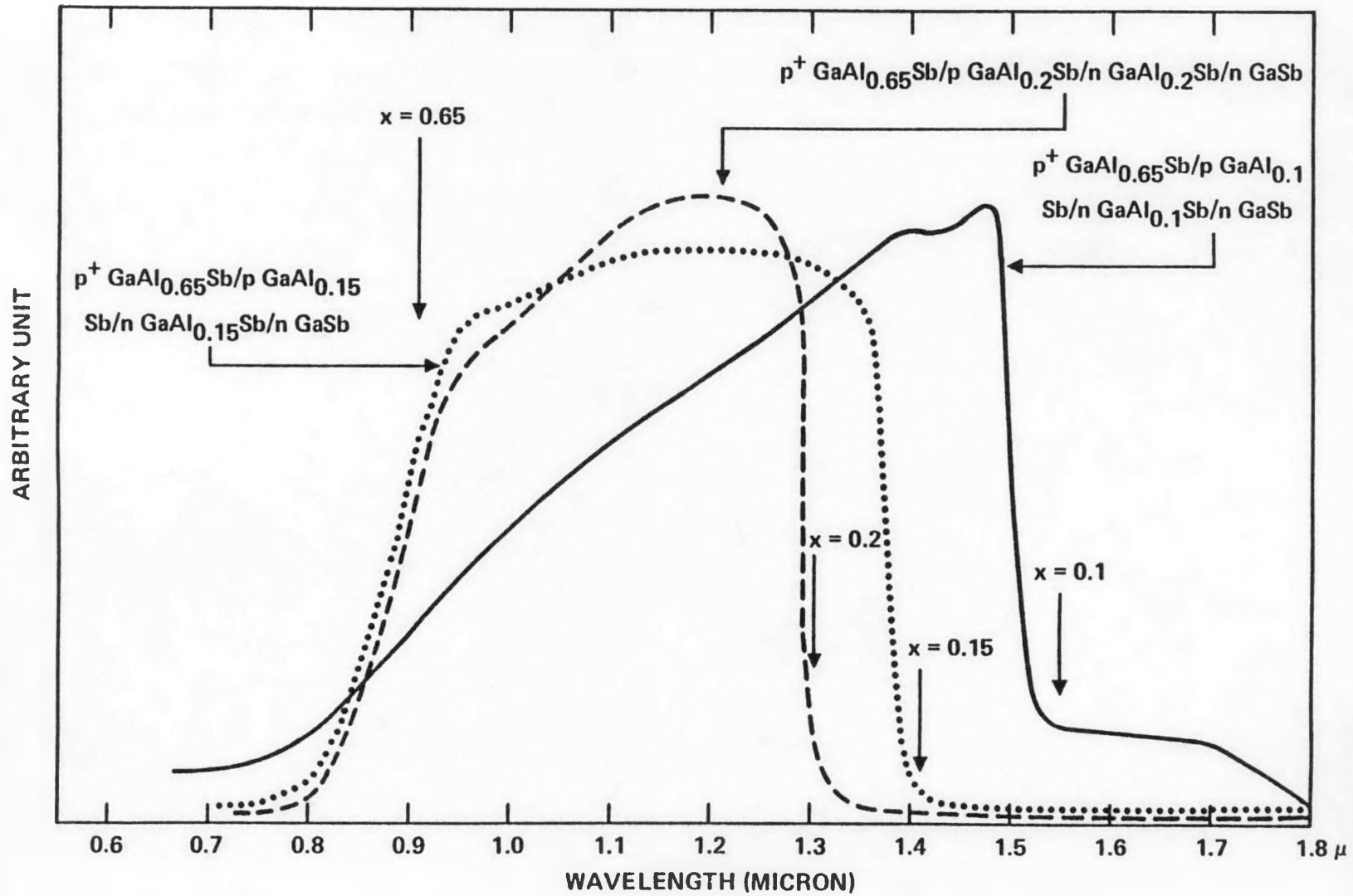
16

Fig. 9. Spectral response curves of heteroface structure with same junction layers but different window layers.

ERC41033.25TPR



Rockwell International



ERC41033.25TPR



Rockwell International

Fig. 10. Spectral response curves of AlGaSb heteroface structures with different junction layers but same window layers.

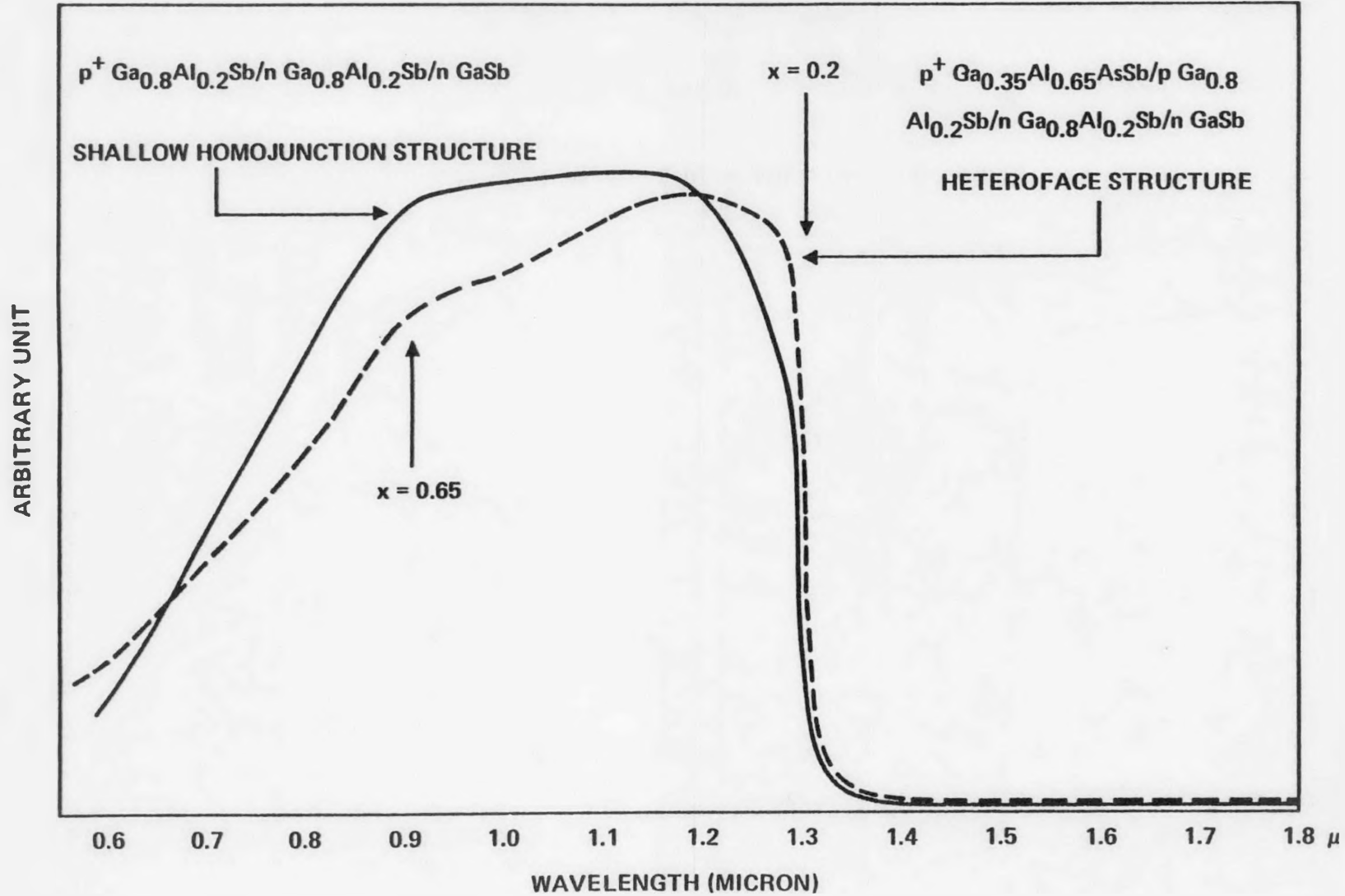


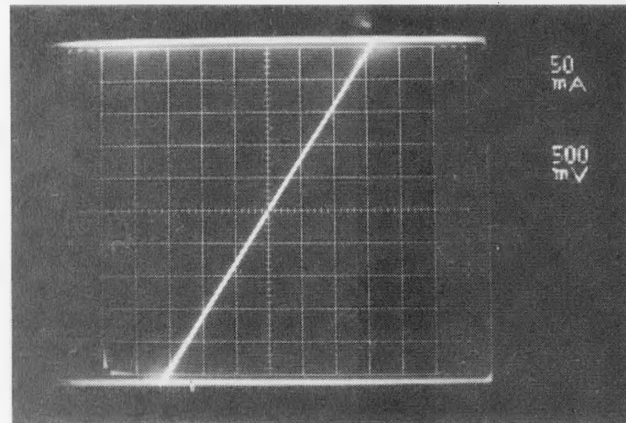
Fig. 11. Spectral response curves of an  $Al_{0.2}Ga_{0.8}Sb$  heteroface cell with 65% Al window layer and an  $Al_{0.2}Ga_{0.8}Sb$  shallow homojunction cell.



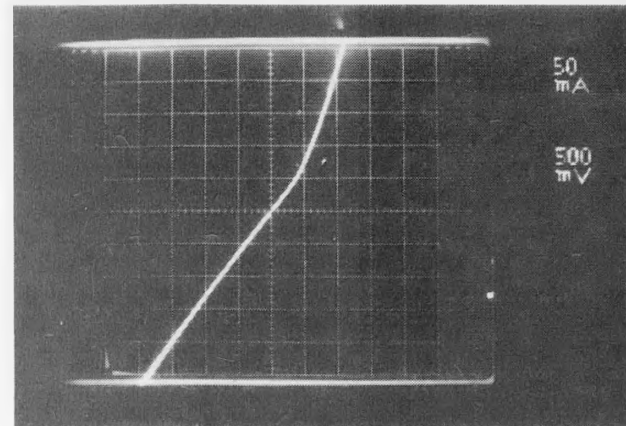
TABLE II

Y-26	$n^+ \text{Al}_{.25}\text{Ga}_{.75}\text{As}/n^+ \text{GaAs}$
Y-29	$p^+ \text{Al}_{.25}\text{Ga}_{.75}\text{As}/p^+ \text{GaAs}$
L-5-2	$p^+ \text{Al}_{.65}\text{Ga}_{.35}\text{AsSb}/p \text{GaSb}$
S-3	$p^+ \text{GaAs}$
S-4	$n^+ \text{GaAs}$

ERC80-9688



(a)



(b)

Fig. 12 Current voltage characteristics of (a) ITO/p<sup>+</sup> Al<sub>0.65</sub>Ga<sub>0.35</sub>AsSb and (b) ITO/n<sup>+</sup> GaAs contacts.



ERC41033.25TPR

The Nd-glass laser to be used for intercell bonding experiments was assembled in this period. However, because of the reorganization of the lab space, the laser has been moved to another lab for the time being. The operation of this laser is expected to start in the next quarter.



## 4.0 DEVICE FABRICATION AND CHARACTERIZATION

### 4.1 Accomplishments

- Complete heteroface  $p^+ Al_{.65}Ga_{.35}AsSb/p Al_{.2}Ga_{.8}Sb/n Al_{.2}Ga_{.8}Sb/n GaSb$  solar cell was successfully fabricated and characterized.
- $p^+/n$  shallow homojunction  $Al_{.2}Ga_{.8}Sb$  solar cell has been fabricated and characterized. Open circuit voltages as high as 0.35 V, 0.55 V and 0.66 V were achieved at 1 SUN,  $\sim 200$  SUNs and  $\sim 1000$  SUNs, respectively.
- Front side ohmic contact experiment has been done during this period for AlGaAs cells. Both Zn and Au might be responsible for the degradation after alloying the contact.

### 4.2 AlGaSb Subcells

The LPE furnace overhaul and modifications in growth technique described earlier have allowed successful growth of  $Al_xGa_{1-x}As_ySb$  subcell structures having windows with Al contents of  $x = 0.65$  and As contents of  $y \sim 0.007$ . The As concentration in the solid is limited to this low value by the As solubility limit in the liquid at the growth temperature. This amount of As is insufficient to provide complete lattice matching to the GaSb substrate or low Al junction layers, but its inclusion is thought to be beneficial in reducing lattice mismatch strains within the structure.

Electrical characterization of subcells fabricated from structures covering a wide range of compositions shows some clear trends: (1) short circuit current density increases with Al content of the window layer (from  $\sim 7 \text{ mA/cm}^2$  for  $x = 0.4$  to  $\sim 11.5 \text{ mA/cm}^2$  for  $x = 0.65$  under simulated 1 SUN AM1 illumination without AR coating, (2) fill factor decreases with increasing Al content of the window when the front surface metallization is applied directly on the window layer.

Illuminated I-V curves typical of heteroface structures having junction layers with  $x = 0.2$  and window layers with  $x = 0.65$  or  $0.4$  are shown in Figs. 13(a) and (b) respectively. The mesa area of these structures is  $0.025 \text{ cm}^2$ .

In an effort to attain high short circuit current along with a good fill factor, attempts were made to construct  $p^+/n$  shallow homojunction  $\text{Al}_{0.2}\text{Ga}_{0.8}\text{Sb}$  solar cells to allow the front contact to be made directly on the low Al junction layer instead of a higher Al window layer. As anticipated, this direct contact appreciably reduced series resistance and enhanced the fill factor from the 0.43 obtained with a 65% Al window layer, or the 0.51 obtained with a 40% Al window layer to 0.61. Figures 14(a) and (b) show the light I-V characteristics of the  $p^+/n$  shallow homojunction  $\text{Al}_{0.2}\text{Ga}_{0.8}\text{Sb}$  cell at 1 SUN and 200 SUNs AM1 respectively. The reduction of fill factor at the higher concentration ratio is primarily due to series resistance in the front contact.

Unfortunately, the  $p^+/n$  shallow junction cell achieved a short circuit current density of only  $5.1 \text{ mA/cm}^2$ . Possible reasons are (1) non-optimum junction depth, and (2) inadequate minority carrier diffusion length in n-type material to maintain good long wavelength response.

The open circuit voltage enhancement with sunlight concentration is encouraging.  $V_{oc}$  increases from 0.355 V at 1 SUN to 0.546 V at 200 SUNs. Under illumination from a camera flash gun providing an intensity of  $\sim 1000$  SUNs, the  $V_{oc}$  reached a value of 0.66 volts. This is indicated in Fig. 15 which shows a typical  $V_{oc}$  vs. time curve recorded for this type of flash illumination condition.

In the last month of this quarter, to further explore the usefulness of shallow homojunction structures, we have attempted to grow  $n^+/p$  shallow homojunction  $\text{Al}_{0.2}\text{Ga}_{0.8}\text{Sb}$  cells with a very thin  $n^+$  layer. However, the junctions were all shorted. This shorting was presumably due to (1) the  $n^+$  layer being too thin to be continuous or (2) the background level of Sb vacancies in the undoped p-layer is too high.



ERC41033.25TPR

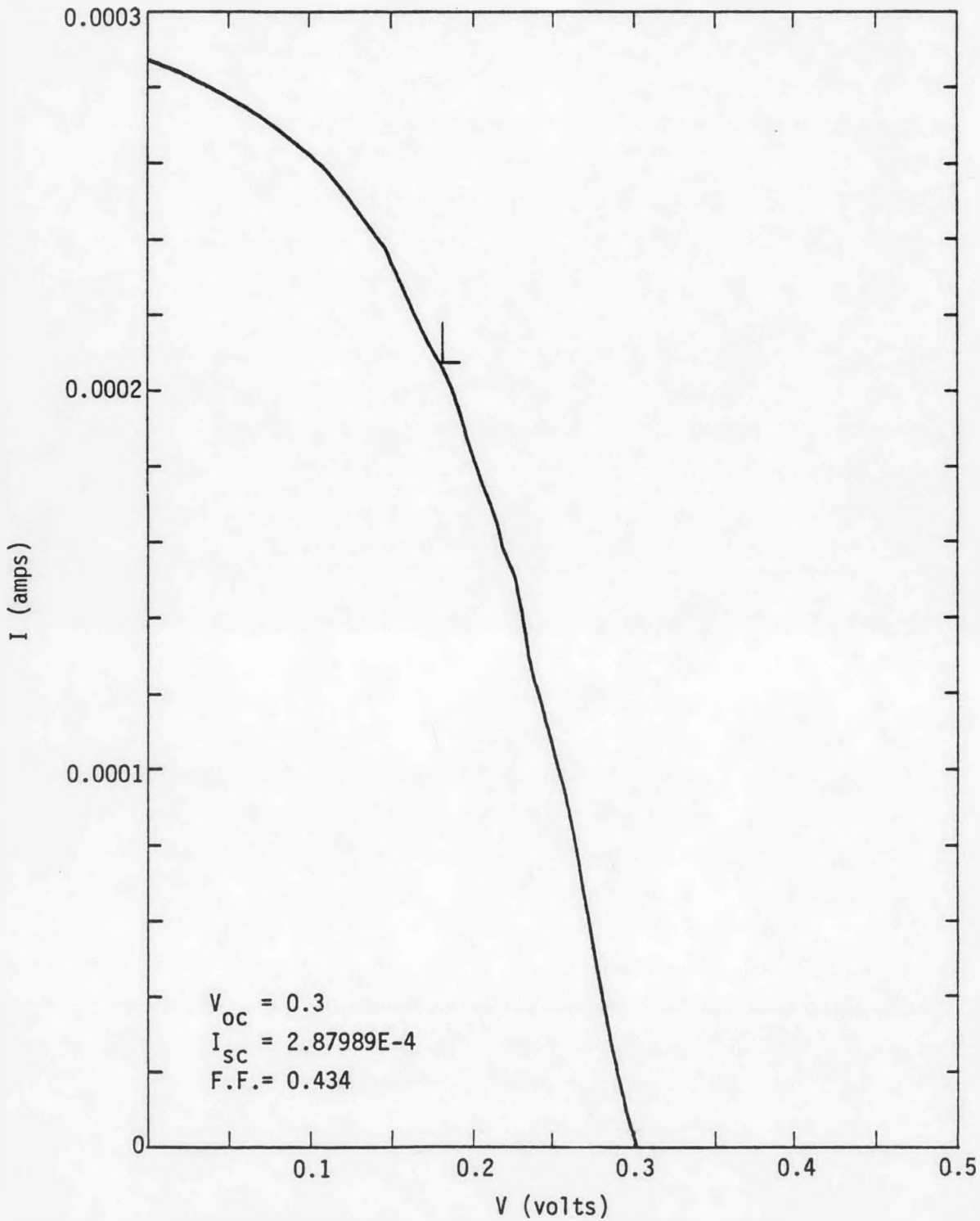


Fig. 13. (a) Light I-V curve for  $p^+ Al_{0.65}Ga_{0.35}AsSb/p Al_{0.2}Ga_{0.8}Sb/n Al_{0.2}Ga_{0.8}Sb/n GaSb$  heteroface cell under simulated 1 SUN AM1 illumination. Front contact made directly to window layer.



ERC41033.25TPR

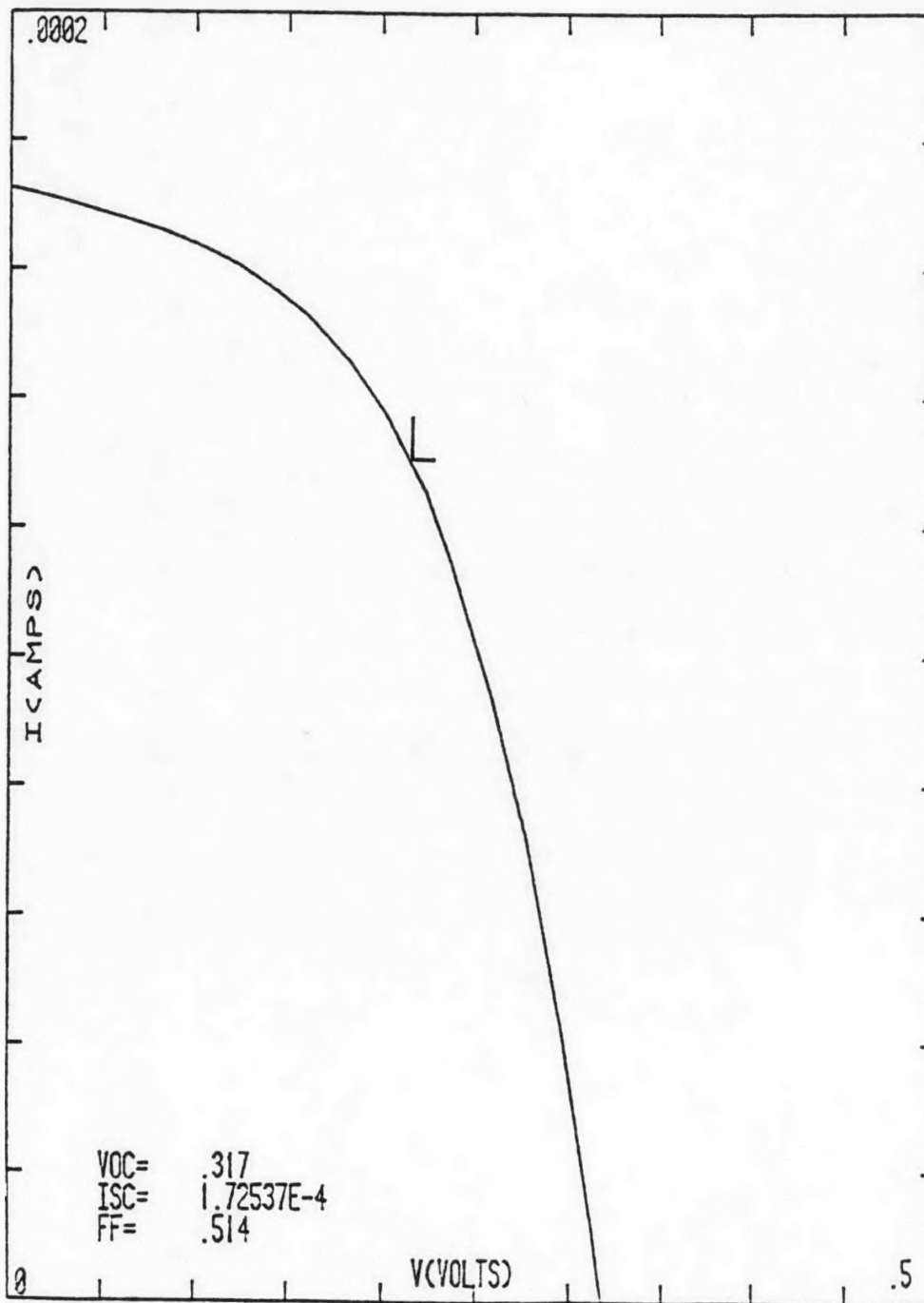


Fig. 13 (b). Light I-V curve for  $p^+ Al_{.4}Ga_{.6}AsSb/p Al_{.2}Ga_{.8}Sb/n Al_{.2}Ga_{.8}Sb/n GaSb$  heteroface cell under simulated 1 SUN AM1 illumination. Front contact made directly to window layer.

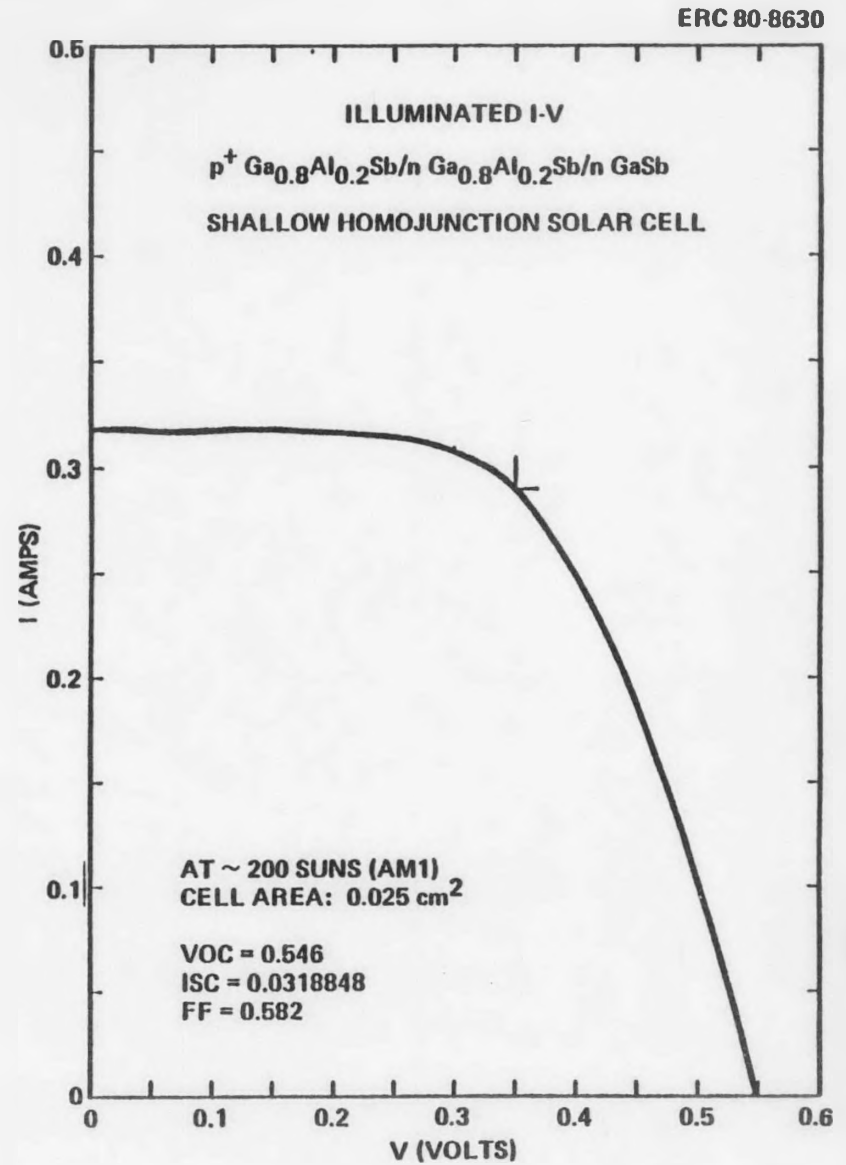
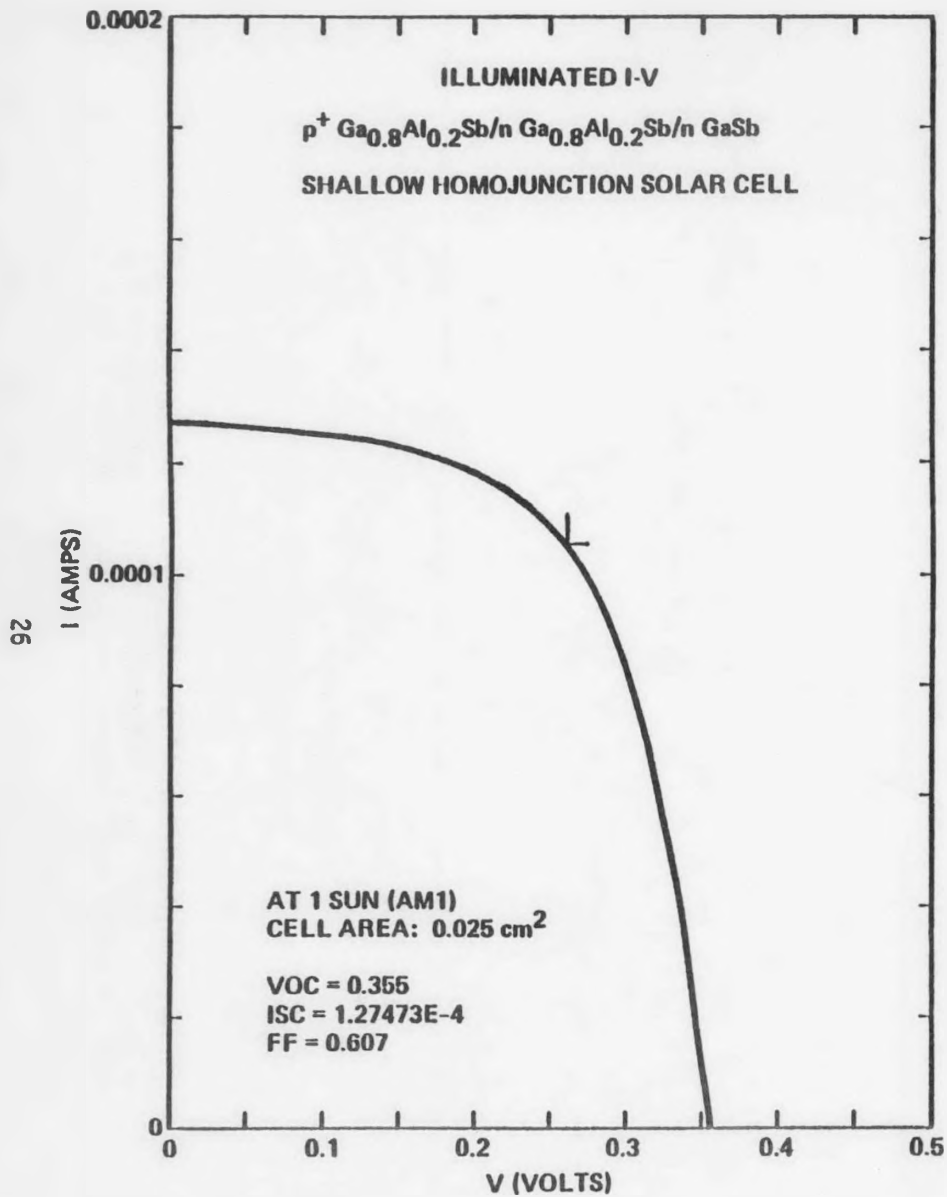


Fig. 14. Light I-V curves for  $p^+ \text{Al}_{0.2}\text{Ga}_{0.8}\text{Sb}/n \text{Al}_{0.2}\text{Ga}_{0.8}\text{Sb}$  shallow homojunction cell under simulated 1 SUN and ~200 SUNS illumination.

ERC41033.25TPR

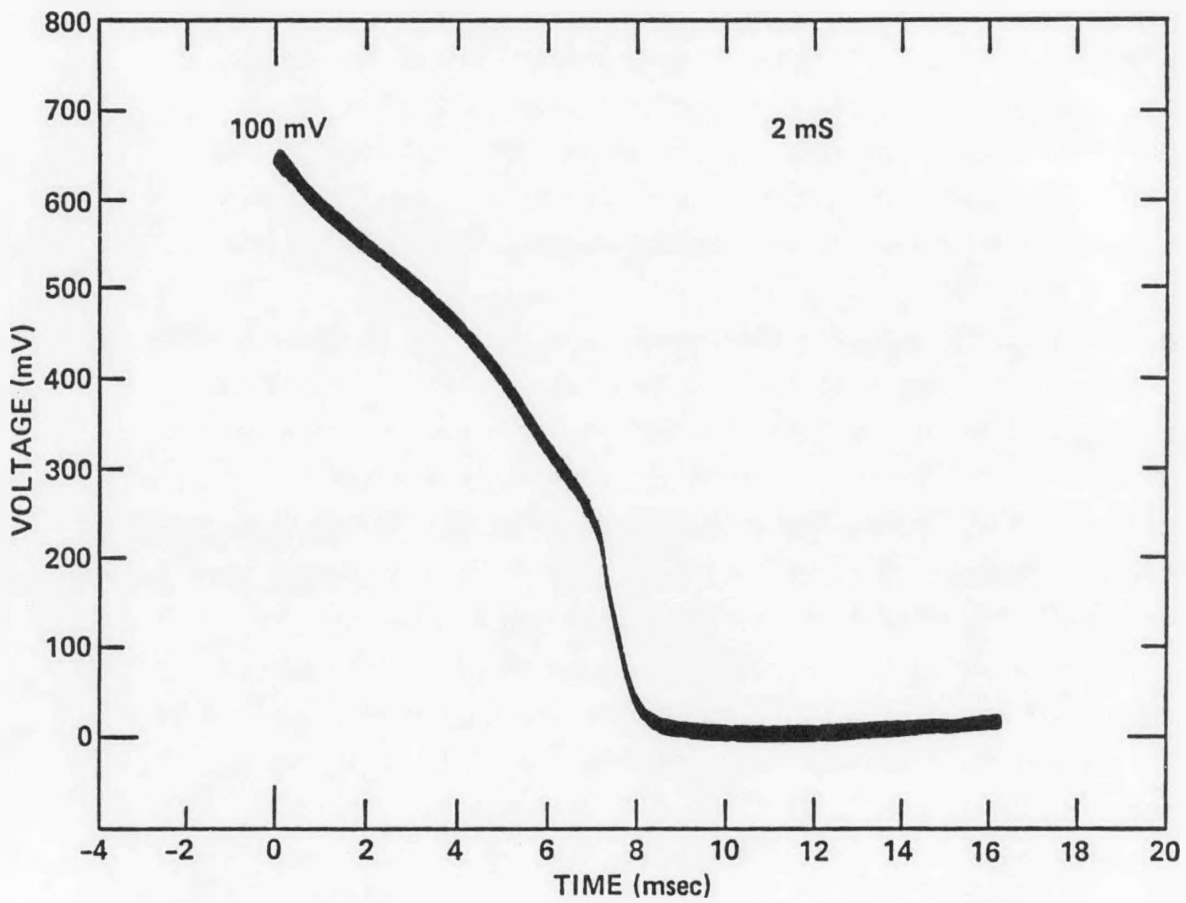


Fig. 15. Open circuit voltage vs. time under a camera flash unit simulated ~1000 SUNs illumination.

In the next quarter, we will keep on trying this  $n^+/p$  structure. We will try to have better control of the  $n^+$  layer thickness and to determine the undoped p-layer doping level by Hall measurement.

#### 4.3 AlGaAs Subcells

Relatively low fill factors have also been a problem for AlGaAs cells, again because of high series resistance between the metal contact and the high Al window layer. Efforts have been made in this period to form low resistance ohmic front contacts, by (1) making direct contact to the low Al junction layer by etching through the window layer, and (2) trying various metal combinations and alloying conditions to avoid metal diffusion into the junction area during alloying.

In the past, for standard GaAs heteroface cells, a 5% HF selective etch which does not appreciably attack GaAs has been used successfully to etch through  $Al_{.85}Ga_{.15}As$  window layers without damage to underlying GaAs junction layers. However, for the present application, where the junction layers are typically  $Al_{.2}Ga_{.8}As$ , the attack tends to be non-selective between window and junction layers. As a result, much greater care in controlling etching parameters is required to avoid junction layer damage.

Figure 16 shows the illuminated I-V curve of an AlGaAs cell in which the contact was directly applied to the low AlGaAs layer. The fill factor was 0.71 prior to alloying. However, both the fill factor and  $V_{oc}$  degraded after alloying at  $400^\circ C$  for  $\frac{1}{2}$  minute. A significant increase in dark current at a given voltage after alloying is apparent from the comparative dark I-V curves shown in Fig. 17. This increased dark current may be due to diffusion of contact metal species (e.g., Zn, Au) to cause partial shunting of the junction.



ERC41033.25TPR

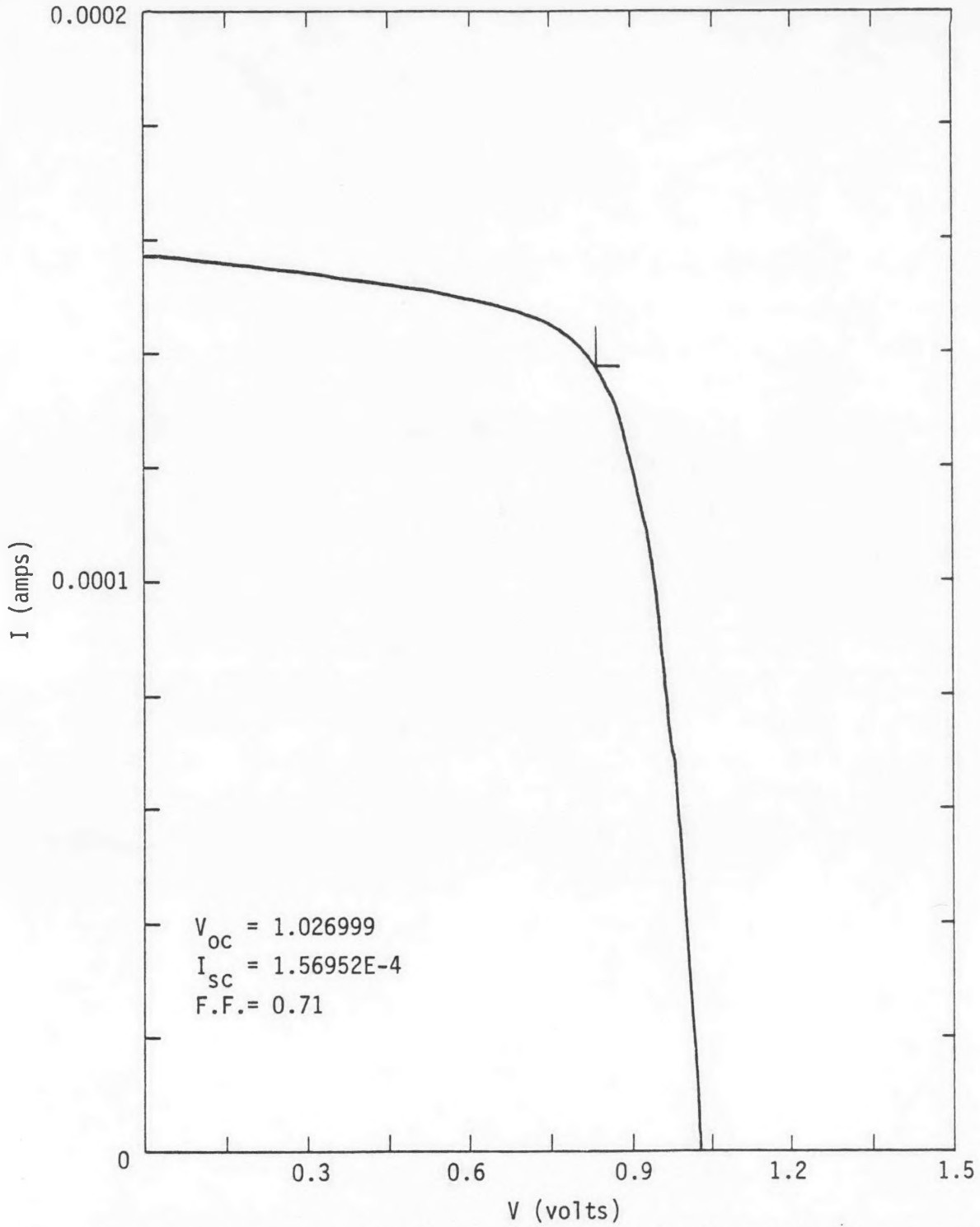


Fig. 16. Light I-V curve for  $p^+ Al_{0.85}Ga_{0.15}As/p Al_{0.35}Ga_{0.65}As/n Al_{0.35}Ga_{0.65}As/n GaAs$  cell under simulated 1 SUN AM1 illumination. Unalloyed Au-Zn front contact applied directly to junction layer.



ERC41033.25TPR

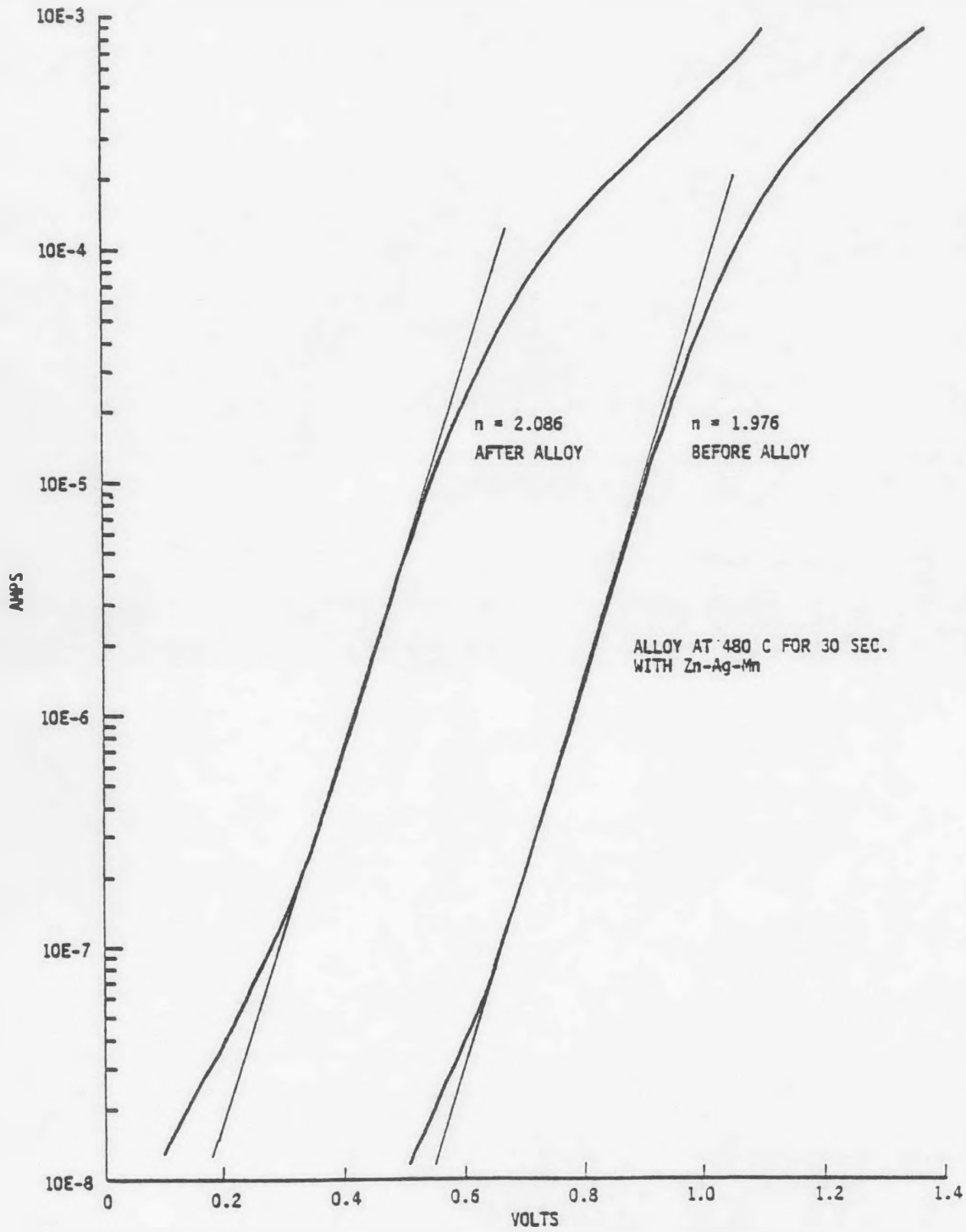


Fig. 17. Dark I-V curves for  $p^+ Al_{0.85}Ga_{0.15}As/p Al_{0.35}Ga_{0.65}As/n Al_{0.35}Ga_{0.65}As/n GaAs$  cell before and after alloying process